npj | parkinson's disease

Article

Published in partnership with the Parkinson's Foundation

https://doi.org/10.1038/s41531-025-00957-6

Characterizing the heterogeneity of neurodegenerative diseases through EEG normative modeling

Check for updates

Judie Tabbal[1], Aida Ebadi[1], Ahmad Mheich[1,2], Aya Kabbara[1,3], Bahar Güntekin[4,5], Görsev Yener[6,7], Veronique Paban[8], Ute Gschwandtner[9], Peter Fuhr[9], Marc Verin[10,11], Claudio Babiloni[12,13], Sahar Allouch[1] & Mahmoud Hassan[1,14]

Neurodegenerative diseases like Parkinson's (PD) and Alzheimer's (AD) exhibit considerable heterogeneity of functional brain features within patients, complicating diagnosis and treatment. Here, we use electroencephalography (EEG) and normative modeling to investigate neurophysiological mechanisms underpinning this heterogeneity. Resting-state EEG data from 14 clinical units included healthy adults ($n = 499$) and patients with PD ($n = 237$) and AD ($n = 197$), aged over 40. Spectral and source connectivity analyses provided features for normative modeling, revealing significant, frequency-dependent EEG deviations with high heterogeneity in PD and AD. Around 30% of patients exhibited spectral deviations, while ~80% showed functional source connectivity deviations. Notably, the spatial overlap of deviant features did not exceed 60% for spectral and 25% for connectivity analysis. Furthermore, patient-specific deviations correlated with clinical measures, with greater deviations linked to worse UPDRS for PD ($\rho = 0.24$, $p = 0.025$) and MMSE for AD ($\rho = -0.26$, $p = 0.01$). These results suggest that EEG deviations could enrich individualized clinical assessment in Precision Neurology.

As the global population ages rapidly, the number of people over 60 is expected to double by 2050. This trend coincides with an expected rise in the prevalence of patients with age-related progressive neurodegenerative diseases, such as Parkinson's (PD) and Alzheimer's (AD) diseases, belonging to cognitive deficits and disabilities in the activities of daily living, culminating in the diagnosis of dementia. Current estimates project that the number of people living with dementia is about 50 million and will triple to 153 million by 2050[1]. Among them, the majority suffer from AD. Furthermore, the number of people with PD is expected to reach around 16 million globally. Notably, there has been no therapy able to cure or stop AD and PD until now, motivating more research on age-related brain changes in pathological aging.

Over the past three decades, advances in neuroimaging and electroencephalographic (EEG) techniques have provided invaluable biomarkers reflecting brain dysfunctions, enhancing efforts to describe aging processes, distinguish between healthy and diseased individuals, and predict disease progression[2–9]. However, most research studies have traditionally focused on MRI and EEG biomarkers derived from group analyses, comparing healthy controls to patient populations or patient populations along the disease course or in response to treatments[10]. However, by averaging data across a population, group analyses tend to obscure individual variations, which can mask important differences in disease progression and response to treatment at individual level[10,11]. According to Precision Medicine, this "*one-size-fits-all*" methodology fails to account for the unique genetic,

[1]MINDIG, F-35000 Rennes, France. [2]Service des Troubles du Spectre de l'Autisme et apparentés, Département de Psychiatrie, Lausanne University Hospital (CHUV), Lausanne, Switzerland. [3]Faculty of Science, Lebanese International University, Tripoli, Lebanon. [4]Department of Biophysics, School of Medicine, Istanbul Medipol University, Istanbul, Turkey. [5]Research Institute for Health Sciences and Technologies (SABITA), Neuroscience Research Center, Istanbul Medipol University, Istanbul, Turkey. [6]Izmir University of Economics, Faculty of Medicine, Izmir, Turkey. [7]Izmir Biomedicine and Genome Center, Izmir, Turkey. [8]Aix Marseille Univ, CNRS-UMR 7077, CRPN, Marseille, France. [9]Departments of Clinical Research and of Neurology, University Hospital of Basel, Basel, Switzerland. [10]Centre Hospitalier Université d'Orléans, Service de Neurologie, Orléans, France. [11]B-CLINE, Laboratoire Interdisciplinaire pour l'Innovation et la Recherche en Santé d'Orléans (LI²RSO), Université d'Orléans, Orléans, France. [12]Department of Physiology and Pharmacology "Vittorio Erspamer", Sapienza University of Rome, Rome, Italy. [13]D San Raffaele Cassino Hospital, Cassino FR, Italy. [14]School of Science and Engineering, Reykjavik University, Reykjavik, Iceland. e-mail: mahmoud.hassan.work@gmail.com

Parkinson's Foundation

environmental, and lifestyle factors that influence each patient's condition. Consequently, treatments based on group data may be less effective or even inappropriate for certain individuals, leading to suboptimal outcomes.

In this context, normative models (NM) emerge as a powerful tool to make individual-level inferences by describing the population norm and then assessing the degree to which each individual deviates from these norms[10–12]. While normative charts are well-established in other domains, such as pediatric growth charts, their application to neuroimaging data is relatively recent. Similar to how growth charts track a child's development by comparing their height and weight to peers, recent MRI studies combined with normative models have endeavored to chart analogous trajectories for brain phenotypes (e.g., gray and white matter volumes, mean cortical thickness, total surface area, etc.) to map lifespan age-related changes in brain structure[13–15] and characterize structural/functional heterogeneity in psychiatric disorders[16–18], schizophrenia and bipolar disorder[19], as well as in neurodegenerative disease as Alzheimer's disease (AD)[15,20–22].

While recent studies have focused on MRI data, the EEG-based normative modeling field remains largely unexplored. Notably, Lefebvre et al. used normative models to investigate variability among autistic patients as compared to healthy controls[23]. More recently, we charted the trajectory of brain development in a population aged between 5 and 18 years and mapped the heterogeneity of psychiatric diseases as reflected in spectral power density spectra computed at scalp electrodes from resting-state eyes-closed EEG activity and cortical source functional connectivity estimated from that activity[24]. In this study, we utilized normative models and EEG data from 14 datasets to achieve two primary objectives. First, we aimed to chart the trajectory of standard EEG features, including EEG relative power and source-level functional connectivity, in a cohort of healthy control (HC) individuals over 40 years old (yo). Second, we leveraged individual-level inferences from the normative models to map the heterogeneity within AD and PD groups.

Results

Data description

Resting-state eyes-closed EEG data was collected from subjects aged 40 to 92 years, across 14 sites (see "Methods"). Normative models were trained on 400 (46% M) HC participants while 99 (42% M) HC participants were held out as a comparison group against the clinical cohort. The clinical groups comprised 237 PD patients (65% M), and 197 AD patients (37% M). An overview of the age distribution across groups, sex, and sites is provided in Fig. 1.

Building the normative model

Using a reference sample of HC individuals, we trained a Generalized Additive Models for Location Scale and Shape (GAMLSS) for each EEG feature (see "Methods"). Specifically, relative EEG power and cortical source functional connectivity values were computed at each scalp electrode/functional connection between cortical source pairs for the frequency bands of interest (i.e., delta, theta, alpha, beta, and gamma) were modeled. The optimal distribution family, model parameters (μ, σ, ν, τ), and covariates are indicated in Supplementary Tables 4 and 5. The performance and robustness of our models are depicted in Supplementary Figs. 3–6. Leveraging our reference healthy cohort, we generated the typical trajectory observed in spectral and functional connectivity features. An example of these normative trajectories at the alpha band is presented in Fig. 2, showcasing the averaged spectral and connectivity features across channels and connections Results across frequency bands can be found in Supplementary Figs. 7 and 8.

Heterogeneity within neurodegenerative diseases

After generating the normative trajectories, we projected individuals diagnosed with PD and AD, alongside an HC test group, onto these models, and derived subject-specific deviation scores. Following previous work done by refs. 14–16,18–20 to quantify within-group heterogeneity, we computed the number of extremely deviated channels (scalp electrodes)/functional source connections ($|z\text{-scores}| > 2$) per participant (Supplementary Figs. 9 and 10) and the percentage of participants with at least one extremely deviated channel/connection (Supplementary Tables 6 and 7).

Results of the spectral analysis showed that the percentages of participants having at least one deviation were relatively low with the highest values occurring at the theta band (PD: 31.36%, AD: 27.41%, *positive deviation*). The values of the negative deviation reached their maximum at the beta band (PD: 12.71%, AD: 23.35%, *negative deviation*), indicating that a good proportion of participants exhibited significant similarities with the HC persons forming the training HC(train) group. The number of channels (EEG power density computed at scalp electrodes) per participant negatively deviating from the normative model was significantly greater for AD compared to HC(test) at the alpha and beta bands ($p < 0.01$, Mann–Whitney test). Compared to the HC individuals, these patients had lower EEG power density at those bands. Regarding positive deviations, both PD and AD groups showed significant differences compared to the HC(test) group at the theta, alpha, and beta bands ($p < 0.05$). Compared to the HC group, these patients had higher EEG power density at those bands.

Unlike the findings from the EEG spectral analysis, we observed an increase in the number of participants exhibiting at least one extreme negative/positive deviation in the EEG cortical source connectivity analysis. Detailed percentages across all frequency bands and disorders are provided in Supplementary Table 7. Figure 3 demonstrates an example of these measures at the theta band. Particularly noteworthy are the percentages of negative extreme deviations in PD across all frequency bands, where they reached 86.86% at the delta band. Interestingly, PD exhibited a greater number of extreme negative deviations compared to HC(test), while AD displayed fewer. Conversely, the PD group had significantly fewer deviated positive EEG connections at source pairs than the HC(test) group across all EEG frequency bands except delta, whereas AD exhibited a significantly higher number of deviated EEG source connections only at the alpha band ($p < 0.05$).

Next, interested in searching for a common deviation pattern within each group, we evaluated the spatial overlap of extreme deviations by calculating the percentage of participants with extreme deviations ($|z\text{-score}| > 2$) at each channel (EEG power density at scalp electrode)/ functional connection at source pairs within each group to create deviation overlap maps (Fig. 4a, b). For the EEG spectral features at scalp electrodes, a certain consistency in spatial locations among individuals within the same group was observed, more prominently within the HC(test) group than within the PD and AD groups, across all frequency bands. Specifically, we noted some deviated channels that are shared by more than 60% of individuals within the same group. These cases correspond to the HC(test) participants evaluated at the alpha and beta bands (negative deviation), as well as the delta and theta bands (positive deviation). More than 60% of the PD patients shared common extremely deviated channels at the theta band (positive deviation). Similar observations were noted in the case of AD patients at the beta band (negative deviation).

We then compared the channel-wise overlap maps between PD and AD groups and the HC group using group-based permutations[16], generating significant overlap maps (Fig. 4c, d). All results were corrected for multiple comparisons using false discovery rate (FDR) ($p < 0.05$). Our results showed that the overlap maps of both clinical groups, PD and AD, differed significantly from the HC(test) group at the delta, theta, and beta bands. In general, PD patients shared several deviating fronto-central channels for EEG power biomarker (e.g., 6 out of 19 channels) at the delta band, and 2–3 deviating central channels at the theta and beta bands respectively. As for the AD group, few channels survived the permutations and correction at the delta band, while some occipital channels at the theta band and 4 out of 19 left temporal parietal channels at the beta band were significant. Results of overlap maps and permutations test for the remaining frequency bands are presented in Supplementary Figs. 11–13.

Regarding the EEG functional source connectivity features, the spatial overlap of extreme deviations across participants with at least one extreme deviation was notably low, not exceeding 25% across all cases and EEG

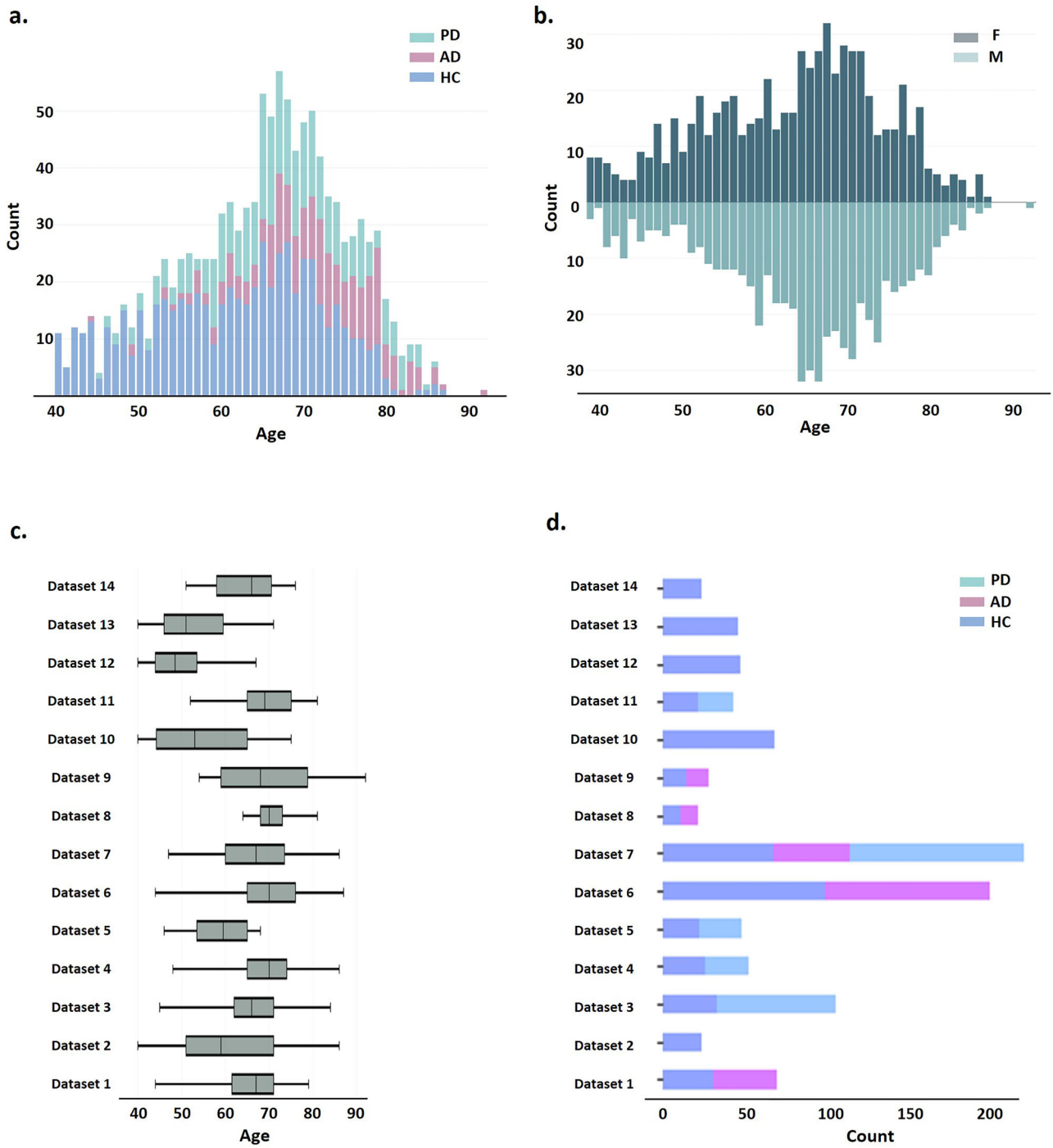

Fig. 1 | Age distribution overview for the whole study. a Age distribution across healthy and clinical groups. **b** Age distribution bar plots across sex for each group (lighter color for female). **c** Age distribution box plots across different sites. **d** Data sample distribution across different sites for healthy and clinical groups.

frequency bands, as shown in Fig. 5. This indicates low consistency in the spatial location of extreme EEG functional source connections among individuals within the same group. Significant differences, detected through group-based permutation tests and corrected using FDR, are illustrated in Fig. 5 for the theta and beta bands and in Supplementary Figs. 14–16 for the other frequency bands. These results illustrate the variations in the overlap maps between clinical (i.e., PD and AD) and HC groups. Notably, only EEG source functional connections with extreme negative deviations survived the permutations and correction tests.

The results revealed that the majority of significantly deviated EEG source functional connections belonged to the default mode network (DMN) network, particularly at the delta (PD: 39%, AD: 44%), theta (PD: 40%, AD: 35%) and alpha (PD: 42%, AD: 44%) bands for both clinical groups. Detailed proportions across resting-state cortical source networks for each clinical group and frequency band can be found in Supplementary Table 8.

Normative model-derived scores as patient-specific markers for clinical assessment

Given the above demonstrated high within-group heterogeneity of the EEG biomarkers used, it is crucial to take into account the participant-specific deviations in any further analysis. Thus, we used the patient-specific

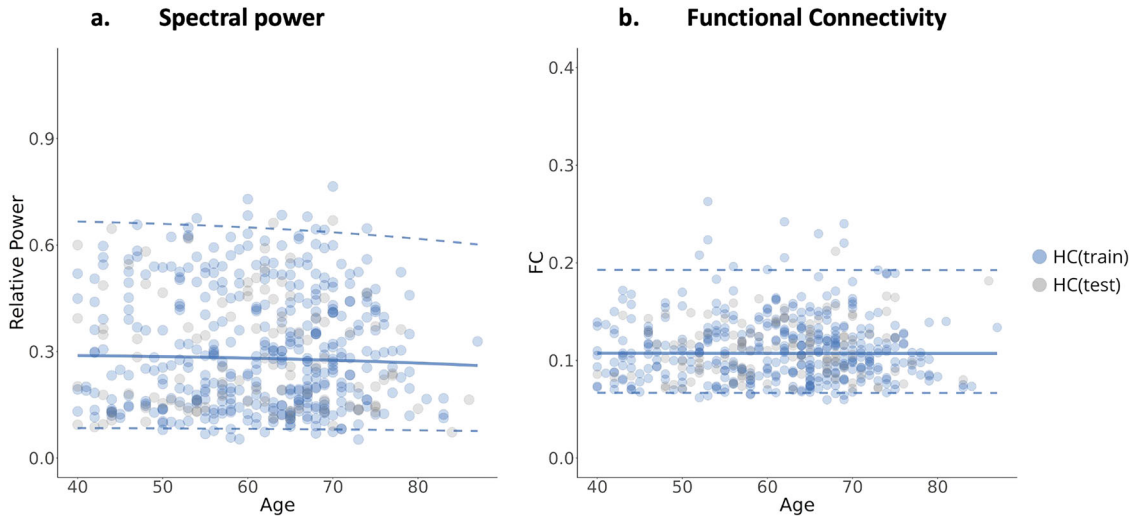

Fig. 2 | Normative aging trajectories of spectral power and functional connectivity in the alpha band. The median (50th percentile) is depicted with a solid blue line, while the 5th and 95th percentiles are indicated by dotted blue lines. **a** NM of the relative power averaged over all channels. **b** NM of FC values averaged over all connections.

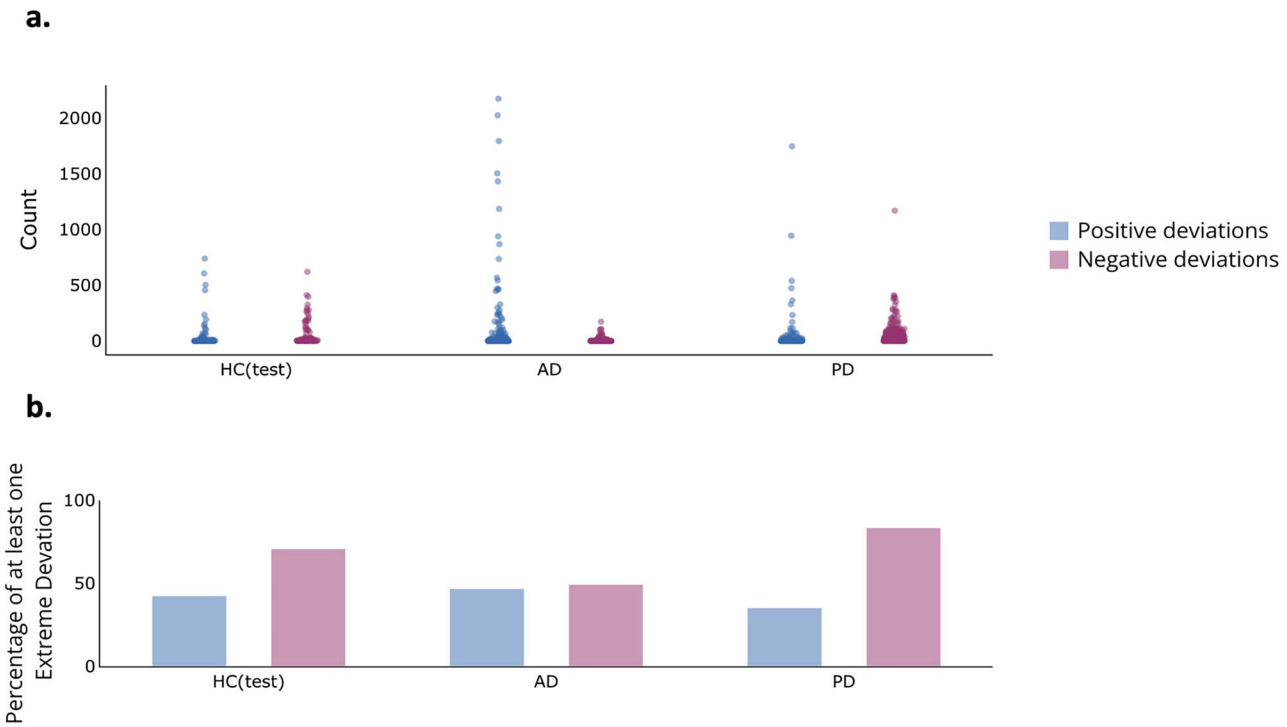

Fig. 3 | Distributions of the extreme deviations in the theta band. a Numbers of extremely deviated connections per subject across groups. **b** Percentages of subjects with at least one extreme deviation per group. Blue (Red) violins represent positive (negative) deviations.

deviations to compute a new metric called EDI (extreme deviations index) defined as the averaged EEG source connectivity of the extremely deviated solutions. This metric was then correlated (Spearman's correlation) with the patients' clinical assessments. For the PD patients, we used their Unified Parkinson's Disease Rating Scale (UPDRS) scores as a clinical assessment measure, and the Mini-Mental State Examination (MMSE) scores as a global cognitive function. UPDRS and MMSE scores were available for a total of 86 and 182 PD patients respectively. Similarly, for the AD patients, we used the MMSE scores, available for a total of 146 AD patients. We found a significant correlation in the delta band for PD patients with UPDRS scores ($\rho = 0.24$, $p = 0.0254$) and AD patients with MMSE scores ($\rho = -0.26, p = 0.0107$), as depicted in Fig. 6. Additionally, for PD patients, a significant correlation with MMSE scores was observed in the delta band ($\rho = -0.35$, $p = 0.0000$), as shown in Fig. 6, and in other frequency bands (alpha and gamma), as presented in Supplementary Fig. 17. We also investigated the correlation between the z-scores of the EDI (z-EDI), representing the averaged z-scores values of the extreme deviations, and found a significant correlation for PD patients with MMSE scores in the theta and beta bands, as shown in Supplementary Fig. 18. These findings represent a preliminary step toward developing EEG-based patient-specific markers that can be used for objectively quantifying personalized treatment modalities.

Discussion

In this study, we aimed to achieve three key contributions. First, we mapped the aging trajectories of the EEG spectral power at scalp electrodes and EEG

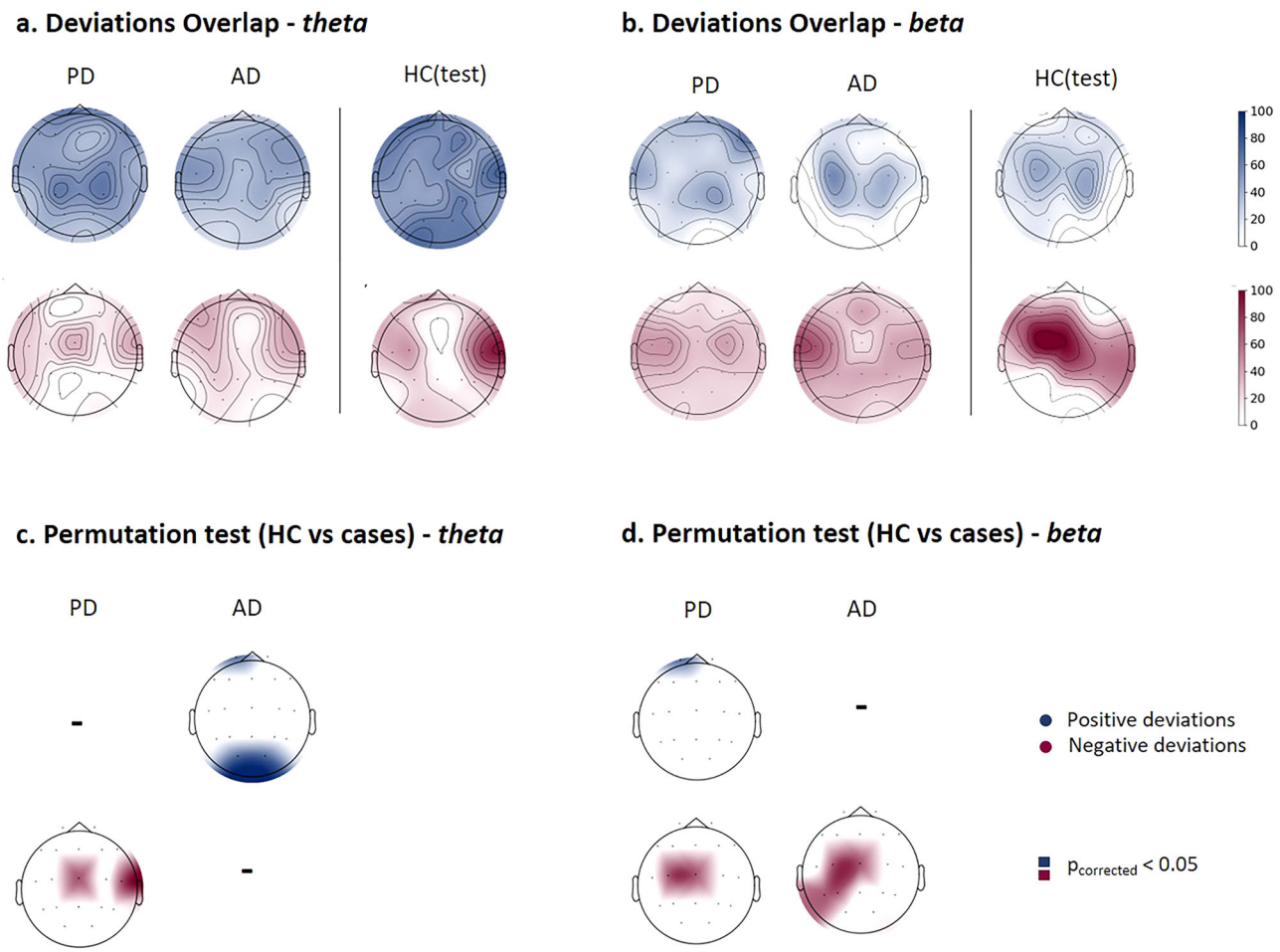

Fig. 4 | Relative power overlap maps. a, **b** Overlap maps of deviation scores for clinical groups and the held-out healthy control group (HC(test)), illustrating areas of common deviation in theta and beta bands respectively. **c**, **d** Significant overlap maps highlighting channels with significant differences between HC(test) and clinical groups, determined by group-based permutation tests ($p < 0.05$, FDR corrected) in theta and beta, respectively.

functional connectivity at cortical source pairs in a HC cohort (>40 yo) as popular neurophysiological biomarkers of interest. Second, we demonstrated the electrophysiological heterogeneity among PD and AD patients, challenging the prevailing reliance on the traditional case-control approach, and emphasizing the importance of acknowledging individual variability. Last, the identification of patient-specific markers derived from normative models showed an association with clinical assessments, which constitutes a preliminary step in developing EEG patient-specific biomarkers for those neurodegenerative diseases with potential applications to other neurodegenerative diseases.

First, we aimed to construct electrophysiological normative aging maps. Thus, we used a normative modeling approach to map the trajectories of EEG biomarkers (features) of interest throughout the >40 yo lifespan, providing a reference model to which individual cases can be compared. As mentioned above, we selected EEG relative spectral power and functional source connectome across standard frequency bands from delta to gamma as response variables for the normative models due to their notable prevalence in the EEG literature[25,26] and the substantial body of research reporting age-related alterations in these features during the process of normal and pathological aging[27–30].

For both EEG features and across all frequency bands, we observed continuous trajectories across age with relatively low variability in averaged EEG functional source connectivity features compared to spectral features. These developmental trajectories suggest that the healthy human brain undergoes gradual development, maintaining a state of stability as individuals' age beyond 40 yo. The slow developmental trajectory observed in our study may be attributed to the brain's adaptive capacity, accumulated knowledge, and lifelong experiences that shape brain function over time[28,31–33].

After constructing the typical aging trajectories from the HC cohort, we sought to elucidate abnormal changes in the electrophysiological aging maps in neurodegenerative diseases. We focused on characterizing the extent to which patient metrics deviate from established norms, thereby providing preliminary insights into the clinical utility of our electrophysiological normative models. Emerging evidence increasingly suggests abnormal alterations in EEG spectral power[27,34–38] and functional connectivity[36,38,39] associated with AD and PD.

Briefly, our results align with previous findings, demonstrating that deviation scores in patients were linked to common channels and connections, as shown by the group-based permutation test. In PD patients, significant overlap was observed in the central lobe across delta, theta, and beta bands, reflecting the involvement of motor-related brain regions, which are crucial for motor control and coordination[40]. This overlap may underscore alterations in motor-related brain regions in PD, providing insights into the neurobiological mechanisms underlying disease's motor symptoms[41]. In contrast, AD patients showed significant patterns in the left temporal-parietal lobes in the beta band, which are interestingly associated with cognitive functions and memory processing[42]. Alterations in these regions may be linked to cognitive decline and memory deficits in AD, with beta-band activity implicated in attention, language, and episodic memory encoding[43], all of which are affected in AD patients. In EEG functional source connectivity, deviations were less spatially consistent across

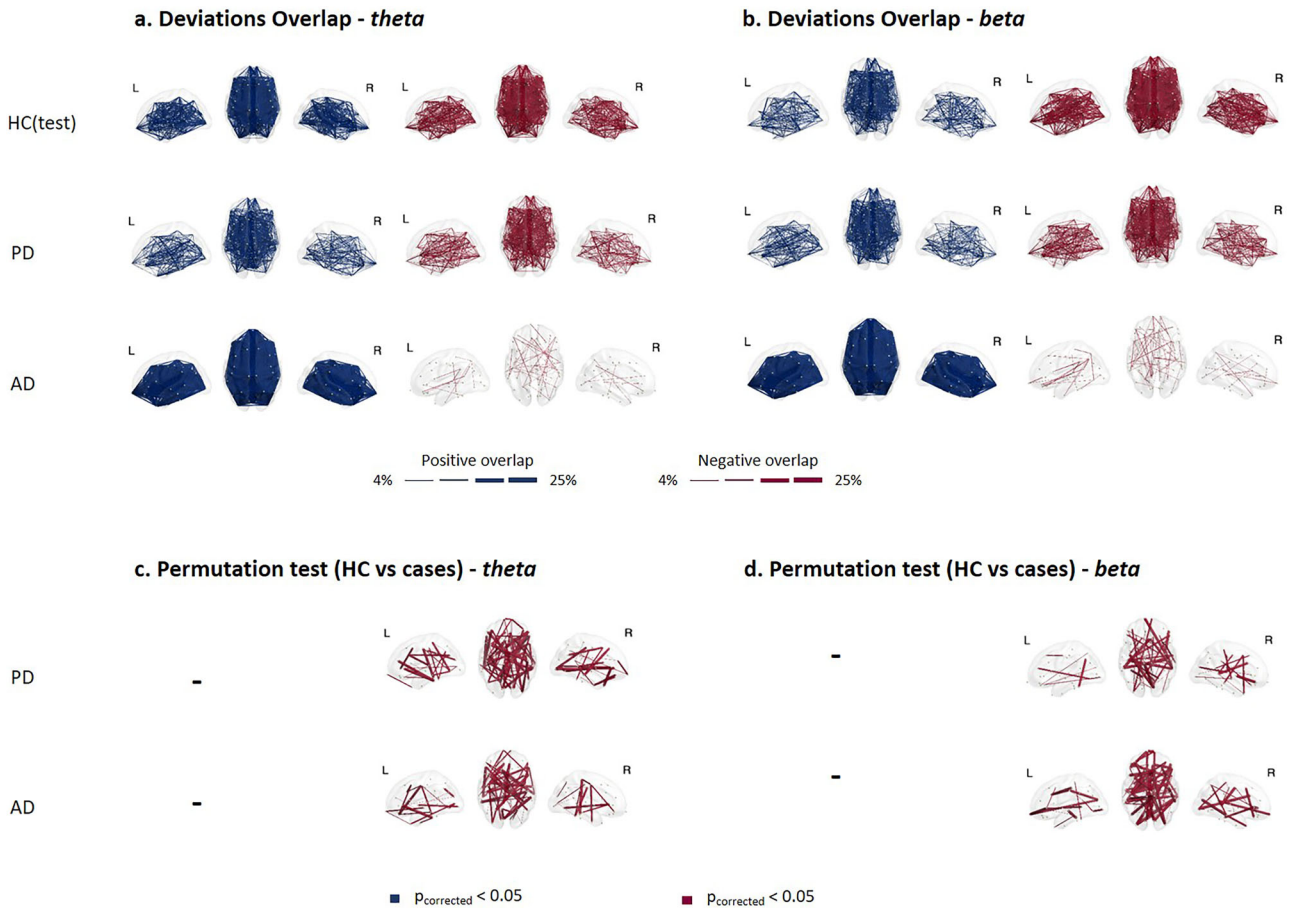

Fig. 5 | Functional connectivity overlap maps. a, **b** Overlap maps of positive and negative deviation scores for clinical groups and the held-out healthy control group (HC(test)) within theta and beta bands respectively, illustrating areas of common deviation among patients. **c**, **d** Significant overlap maps of functional connections showing significant differences between HC(test) and clinical groups at theta and beta bands, determined through group-based permutation tests ($p < 0.05$, FDR corrected).

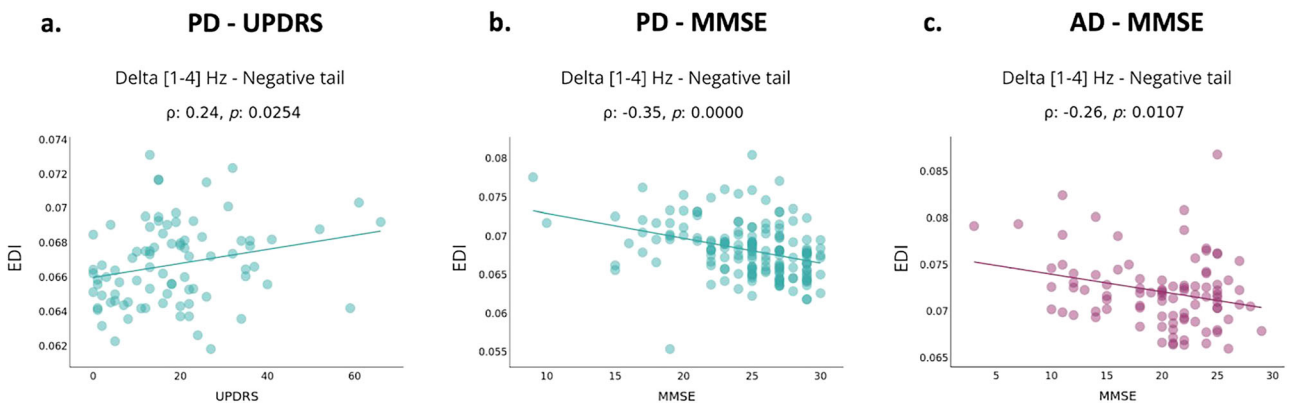

Fig. 6 | NM-derived scores for clinical assessments. a Correlation between PD subjects' "EDI" and UPDRS in the delta band for negative extreme deviations. **b** Correlation between PD subjects' "EDI" and MMSE in the delta band for negative extreme deviations. **c** Correlation between AD subjects' "EDI" and clinical assessment scores (MMSE) in the delta band for negative extreme deviations.

participants but predominantly involved the default mode network (DMN) and dorsal attention network (DAN) networks for both clinical groups across frequency bands. Based on the comprehensible review[44], research work has documented disruptions within these networks in the context of neurodegenerative diseases, reflecting their pivotal roles in cognitive processing and their susceptibility to age-related pathological changes.

Despite the considerable body of research on the induced alterations in EEG features associated with AD and PD, findings across studies lack consistency. Specifically, studies focusing on AD patients have reported examples of inconsistencies in resting-state EEG functional source connectivity literature[39]. This variability may be attributed to the lack of a standardized methodology for EEG acquisition and functional analysis, as well as the reliance on dataset samples that may compromise the results' generalizability. We think that a primary contributor to this inconsistency arises from the inherent heterogeneity among patient populations affected by PD and AD (and other neurodegenerative diseases), which introduces

confounding factors often inadequately addressed in group-level analyses. For instance, despite the general trend of EEG power density shift from higher to lower frequency bands observed in neurodegenerative disease groups compared to HC controls, as outlined in recent systematic reviews[36,37], numerous studies have revealed individual heterogeneity among patients with aging pathologies[45–49]. The main contributors to this substantial heterogeneity are phenotypic diversity, reflecting disease subtypes, and temporal variability, including various disease stages, sex, education attainment, and several endogenous and environmental disease risk factors[50,51]. In our study, the identified heterogeneity in aging EEG functional patterns, characterized by an overlap below 25% for the deviated EEG functional source connectivity measures, aligns with recent findings from investigations that utilized structural MRI and normative modeling in aging cohorts. Indeed, it was shown that spatial patterns of cortical thickness were heterogeneous among AD patients, with overlapping outliers at the regional level not exceeding 50% within the AD group[20]. We believe that the demonstrated heterogeneity poses a significant barrier to the development of EEG-based biomarkers. The challenge associated with the group-level analysis manifests across multiple levels. At the diagnostic level, patients are typically categorized into distinct groups, assuming uniformity within each group. Similarly, treatment approaches often adopt a general "*one-size-fits-all*" strategy, overlooking individual differences. To tackle this issue effectively, the development of patient-specific electrophysiological biomarkers is imperative.

It is noteworthy to highlight the variability observed within the healthy test cohort. Although the healthy test subjects generally showed minimal deviations from the normative model, some individuals exhibited deviations even greater than those observed in the clinical groups (Supplementary Table 6). This reflects the inherent heterogeneity within the healthy population, where individual differences in brain activity can be substantial. Such variability underscores the need for individual-based analyses rather than group-level comparisons, as it allows for a more accurate understanding of brain function across both healthy and clinical populations. Future studies should consider personalized approaches to better capture these individual differences and their implications for both health and disease.

On the other hand, it is crucial to recognize that the differentiation between neurodegenerative diseases, particularly during early and middle stages, poses a significant challenge in clinical practice due to overlapping clinical symptoms across different conditions[52]. In particular, individuals with mild cognitive impairment (MCI) may share common clinical and neurophysiological profiles among aging pathologies, adding complexity to capturing the nuanced variations between conditions[53]. Our work addresses this challenge by generating electrophysiological aging trajectories and leveraging normative models to derive patient-specific deviation scores, which may offer a refined clinical approach compared to traditional methods relying solely on raw features. In the framework of Precision Medicine, the patient's assessment is aimed at not only providing a clinical diagnosis by proper in-vivo biofluid or neuroimaging techniques measuring disease-specific neuropathological species in the brain of PD or AD patients (e.g., amyloid-beta and tau in AD patients), but also to use reliable and valid biomarkers accounting for neurobiological, neuroanatomical, and neurophysiological underpinnings of the individual clinical manifestations along the disease course. Along this line, here we proposed normative models and neurophysiological measures of deviance from resting-state EEG rhythms reflecting specific alterations in the regulation of quiet vigilance in PD and AD patients that are quite relevant to the quality of life of patients (e.g., watching TV programs, reading books and newspapers, having quiet social conversation, etc.)[54].

It is noteworthy to mention that our clinical dataset comprises AD and PD patients with MCI. For example, Dataset 7 includes 38 PD patients with MCI as well as 13 AD patients with MCI. However, the subtype distribution of patients in other datasets is not explicitly stated, potentially including cases of dementia and MCI. As part of our future endeavors, we aim to elucidate patient data regarding subtypes further and use deviation scores derived from the normative models to distinguish between subtypes within each disease, motivated by the work of Young et al., who sought to develop a machine learning tool that enables the discovery of disease subtypes and stages for precise medicine in neurodegenerative disorders[51].

Furthermore, a primary objective of combining EEG and normative modeling is to establish a patient-specific marker with clinical utility. Assessing whether extreme deviations in functional metrics are associated with symptom severity or cognition is crucial. In this study, we examined the clinical correlates of extremely deviated FC features and demonstrated significant associations between individual-specific deviations and clinical assessments for neurodegenerative diseases. Interestingly, the most significant correlation results were observed in the delta band, which is notably associated with brain dysfunction during resting-state conditions and, consequently, cognitive impairment in neurodegeneration[55]. Thus, normative models hold promise for the development of personalized electrophysiological approaches.

In conclusion, the relevance of the observed deviations from healthy controls is twofold: first, by quantifying heterogeneity through overlap maps, we capture individual variability within each disease, highlighting the need for personalized techniques in future studies; second, patient-specific biomarkers derived from these deviations demonstrate significant correlations with clinical scores, advancing toward tailored diagnosis and treatment based on normative models.

Several limitations warrant further consideration. First, while our sample size is substantial for EEG studies ($n \sim 933$), it does not reach the scale often seen in the most important international MRI and fMRI initiatives, and it may not be fully representative of the general population. Notably, in this study, EEG data collected from HC participants primarily fall within the age range (60–70 years), with a notable lack of EEG data above 72 years (see Fig. 1). Further efforts should incorporate additional neuroimaging cohorts to achieve a more balanced representation of individuals across diverse age ranges. We anticipate that EEG-based aging maps established herein will serve as a dynamic resource, with ongoing updates to the electrophysiological aging model as more resource data sets become available. We will specifically focus on integrating longitudinal datasets for a precise characterization of aging developmental trajectories.

Our data was gathered from 14 distinct spontaneous EEG studies, each using different EEG systems with varying spatial resolutions (19, 32, 64, 128, 256 channels) and protocols that were not harmonized. To standardize our analysis for scalp spectral analysis of EEG activity, we mapped all systems to a common low spatial resolution (19 channels). While this approach minimize variability across datasets, it may overlook some relevant information available from higher spatial resolution setups[56]. Moreover, the optimal number of channels required for reliable estimation of functional networks remains an open question, with some studies suggesting that at least 64 channels may be necessary for robust source reconstruction[57]. Furthermore, the use of different EEG systems with varying technical specifications and calibration standards could introduce some variability. Although our preprocessing pipeline and the choice of metrics less sensitive to amplitude differences addressed this issue to some extent, it remains a limitation. Future research should explore advanced harmonization techniques, such as Combat family methods to further enhance compatibility across diverse EEG systems[58]. Moreover, sample sizes varied across datasets. However, to address this issue and identify potential bias arising from individual datasets, we ran a leave-one-study-out analysis. Results showed that no specific dataset significantly influenced NM trajectories (see Supplementary Figs. 5 and 6). Another methodological limitation was the use of fixed EEG frequency bands for delta, theta, and alpha despite the recommendations on the spectral analysis of resting state EEG rhythms by expert panels of the International Federation of Clinical Neurophysiology and The Alzheimer's Association International Society to Advance Alzheimer's Research and Treatment[55,59,60]. These recommendations are based on the evidence that compared to HC persons, AD and PD patients have a remarkable frequency slowing of EEG alpha rhythms (even more pronounced in PD than AD patients), suggesting the use of individual alpha frequency peaks as a landmark to define delta, theta, and alpha frequency

bands. In the present study, we preferred to use standard frequency bands for delta, theta, and alpha rhythms to allow a more direct comparability with the large majority of the EEG literature on PD and AD. Moreover, while this study focused on scalp-level frequency analysis and source-space connectivity due to their established relevance in neurodegenerative disease research, we aim to incorporate source-space spectral power analysis in our future studies to provide a more integrated perspective.

Another challenge of the study arises from the inherent heterogeneity within patient groups, with individuals exhibiting different stages of PD and AD diagnosis. For instance, many datasets lack sufficient information to confirm whether PD or AD patients were at MCI or dementia stages. Therefore, we focused on examining disease-related electrophysiological normative model metrics, regardless of the disease stage. Moreover, this study did not include biomarker data (e.g., cerebrospinal fluid (CSF) analysis, amyloid PET scans) for neurodegeneration diagnoses, which were based on clinical criteria. This reflects a limitation of multi-center EEG datasets and highlights the need for future biomarker-integrated studies for enhanced diagnostic precision.

Additionally, this study did not comprehensively investigate correlations between EEG findings and clinically relevant variables, such as symptom profiles, age of onset, illness duration, medication exposure, or disease severity across disorders. However, we partially explored the influence of medication on EEG results within the patient cohort. While our primary aim was to identify underlying neurobiological patterns, it is important to acknowledge that medication effects may have contributed to variability in the findings. Given that 92% of PD patients (218 out of 237) were ON medication during EEG recordings, we assumed that medication effects were inherently reflected in our analyses, and the outcomes represent the PD patients' typical daily conditions with medication intake. To further address this, we conducted exploratory analyses for the PD group, as detailed in the Supplementary Materials (Supplementary Table 9 and Supplementary Figs. 19–22). These analyses showed no significant differences in z-score deviations for spectral and functional connectivity features between ON/OFF-medication and ON-only conditions, nor between OFF-medication and a matched subset of ON-medication patients. However, the limited sample size of OFF-medication patients restricts the generalizability of these findings. Future studies are warranted to further explore these relationships to gain deeper insights into the clinical and therapeutic significance of the results. Incorporating medication status as covariates in normative models will be essential to better account for pharmacological effects and individual variability.

One limitation of our study is that some datasets included only 19 channels, which may introduce some variability. The optimal number of channels required for reliable estimation of EEG functional networks remains an open question. Several studies have shown that some source reconstruction/connectivity methods require at least 64 channels for robust estimation[57,61]. Nevertheless, this does not affect the overall conclusions of the study, as the high heterogeneity was observed not only at the scalp level but also at the source-space in datasets with high-density EEG.

In addition, it is recommended for future studies to consider the diversity of environmental factors as covariates in normative modeling, particularly given that data is collected from multiple sites with different socio-economic statuses and education levels, which may influence brain aging trajectories.

In conclusion, this study utilized popular resting-state EEG biomarkers and normative modeling to delineate the typical aging trajectories of EEG spectral power and cortical functional source connectivity features and explore the electrophysiological heterogeneity in PD and AD patients. Our findings revealed significant variability in those EEG features among patients, with deviations from normative trajectories correlating with the clinical severity. These findings emphasize the emergent need for patient-level inferences to enhance the accuracy of the neurophysiological assessment in PD and AD patients and inform more personalized treatment strategies. Further research and clinical validation will be necessary to realize these potential benefits fully.

Methods

Datasets

Our cohort consisted of 933 individuals, subdivided into a group of healthy controls ($N = 400$ in the training set, $N = 99$ in the held-out testing set) and a group of 434 participants clinically diagnosed with neurodegenerative disorders, including PD ($N = 237$), and AD ($N = 197$). All participants were aged above 40 years old (mean = 64.95 ± 10.28; 48% M) and underwent resting-state EEG recordings with their eyes closed. For subjects with multiple sessions/runs, only the first session/run was included. The data were aggregated from 14 distinct studies, each approved by its local ethics committee, with informed consent obtained from participants or their legal guardians. For more details about ethics approval, please refer to Supplementary Data 1. The diagnostic criteria used for AD and PD were based on widely accepted standards, such as National Institute of Neurological and Communicative Diseases and Stroke/Alzheimer's Disease and Related Disorders Association (NINCDS-ADRDA)[62] and Diagnostic and Statistical Manual of Mental Disorders (DSM)[63] for AD, and United Kingdom Parkinson's Disease Society Brain Bank (UKPDSBB)[64] and Movement Disorder Society (MSD) criteria[65] for PD. A detailed overview of the datasets—including participants demographics, EEG systems used, data collection sites, selection and diagnostic criteria, available medication information, and references for data access/publication—is provided in Supplementary Data 1. For age distribution across groups, sex, and sites, please refer to Fig. 1.

Data preprocessing

The EEG preprocessing and artifact removal pipeline employed a multi-stage and automated algorithm, supported by visual inspection. Initially, EEG signals underwent bandpass filtering (1–100 Hz). All data signals were downsampled to a common frequency (200 Hz), except for dataset 12, which was originally sampled at 160 Hz and included without resampling as it was added after the preprocessing of other datasets. A notch filter was applied to target the dataset-specific line frequency. Bad EEG channels were identified using the *pyprep* algorithm, which employs a *RANSAC*-based approach, and interpolated based on neighboring electrode data[66]. *RANSAC* selects a small group of EEG channels, estimates a model based on these channels, and then identifies potential outliers or bad channels. Next, re-referencing was applied using the common average reference method to minimize noise across electrodes. Eye blink artifacts were identified and rejected using Independent Component Analysis (ICA) the *IClabel* algorithm[67]. A second bandpass filter (1–45 Hz) further refines the data. Then, EEG signals were segmented into 10-s epochs as a trade-off between the needed length for computing the connectivity matrices and the available segment length per site, and the *Autoreject* toolbox[68] was used to detect and clean or reject bad epochs. All EEG datasets underwent the same preprocessing steps described here, except for dataset 3 (*BASEL*), which was already preprocessed as detailed in refs. 69–71.

Scalp-level spectral features

The normative model establishes the relationship between a response variable and one or more covariates. In this study, we initially focused on the spectral features of the EEG signal as the designated response variable. This choice was motivated by the extensive literature highlighting the changes in EEG power associated with neurodegenerative diseases[34,36,37,72]. The power spectrum density (PSD) for each epoch and each channel is computed using Welch's method (1-s *Hann* window with a 50% overlap, and a spectral resolution of 0.5 Hz). PSDs are then averaged across all epochs within a subject. Relative power in specific frequency bands (delta [1–4 Hz], theta [4–8 Hz], alpha [8–13 Hz], beta [13–30 Hz], gamma [30–45 Hz]) is computed by dividing the absolute power within each narrow band by the total power of the broader band [1–45 Hz]. For scalp-level spectral analysis, we downsampled the electrode configurations to a common 10–20 montage to account for the variability in the number of channels across datasets. We used the "Nihon Kohden EEG 2100" as the reference because it has the minimal number of channels (19 electrodes) among the systems used, and represents a widely accepted standard in clinical and research EEG studies.

The mapping between the Nihon Kohden and other EEG systems was based on the name and/or coordinates of the channels. Subsequently, the spatial alignment of electrodes was visually inspected across datasets to ensure consistency. A detailed mapping of channel indices is provided in Supplementary Data 2.

Source-level functional connectivity features

We computed EEG-based functional networks using the EEG source connectivity method[73]. Cortical sources were estimated using the exact low-resolution brain electromagnetic tomography (eLORETA)[74]. The noise covariance matrix was set to an identity matrix and the regularization parameter was fixed at $\lambda = 0.1$. Age-specific head models of the brain, skull, and scalp layers were built using an MRI template of elderly individuals aged 65–69 years[75], employing the Boundary Element Method (BEM) from the MNE Python package. The forward and inverse models were solved within a source space of 4098 sources per hemisphere, with approximately 5 mm spacing. For the source reconstruction and functional connectivity estimation, we used the full channel count available in each dataset, ensuring that all available information was included. We then downsampled the source space to 68 representative sources by averaging the sources within each region defined by the Desikan-Killiany atlas[76]. Subsequently, we computed the functional connectivity between pairwise regions of interest, using the amplitude envelope correlation (AEC) method, defined as the Pearson correlation between signals' envelopes derived from the Hilbert transform[77,78]. To mitigate zero-lag signal overlaps caused by spatial leakage, we applied a pairwise orthogonalization approach before computing connectivity[79].

Normative modeling

Normative modeling (NM) aims to establish a normative relationship between a response variable (behavioral, demographic, or clinical variables) and at least one covariate (a quantitative biological measure, e.g., age or sex). To estimate the normative age-related curves for EEG spectral power and functional connectivity (as response variables), we implemented the Generalized Additive Models for Location, Scale, and Shape (GAMLSS)[80] using the *gamlss* package. We started by identifying the optimal data distribution and best-fitting parameters and covariates. Utilizing these specific GAMLSS models, we obtained nonlinear normative trajectories for each feature and at each frequency band. The model performance was assessed by the model convergence, residuals, and Q-Q (quantile-quantile) plots. The model sensitivity was analyzed with a leave-one-study-out (LOSO) analysis. Leveraging these population-level normative trajectories, we established benchmarks for each subject using individualized deviation scores.

GAMLSS are semi-parametric regression models offering a flexible framework for capturing complex relationships[81]. They assume a specific distribution for the response variable, with parameters linked to a set of explanatory variables through linear or nonlinear predictor functions. The mathematical formulation of GAMLSS is as follows:

$$y \sim F(\mu, \sigma, \nu, \tau) \tag{1}$$

$$g_\mu(\mu) = X_\mu \beta_\mu + Z_\mu \gamma_\mu + \sum_i s_{\mu,i}(x_i) \tag{2}$$

$$g_\sigma(\sigma) = X_\sigma \beta_\sigma + Z_\sigma \gamma_\sigma + \sum_i s_{\sigma,i}(x_i) \tag{3}$$

$$g_\nu(\nu) = X_\nu \beta_\nu + Z_\nu \gamma_\nu + \sum_i s_{\nu,i}(x_i) \tag{4}$$

$$g_\tau(\tau) = X_\tau \beta_\tau + Z_\tau \gamma_\tau + \sum_i s_{\tau,i}(x_i) \tag{5}$$

The response variable y follows a distribution F defined by parameters (μ, σ, ν, τ). Each parameter is linked to explanatory variables via the link function $g()$, where β represents the fixed effect term and X is its design matrix. γ accounts for the random effects, and Z is its design matrix. s denotes the non-parametric smoothing function[13,81]. In this study, our response variable is an EEG-derived feature, and age serves as the main covariate. The inclusion of other covariates such as sex and data collection sites is detailed in subsequent sections. Following Bethlehem et al., we used fractional polynomials as a smoothing function to accommodate non-linearity while maintaining model stability[13].

The GAMLSS framework provides an extensive range of distribution families. Here, we used an empirical approach to determine the most suitable distribution, by training models across all considered distribution families (with 3 or more moments, continuous/mixed), and comparing them using the Bayesian Information Criterion (BIC). The distribution with the lowest BIC score was selected. This process was systematically applied to the two features under study. The distributions that best fit the averaged spectral power and connectivity values are reported in Supplementary Tables 4 and 5, respectively. In addition, we determined the optimal number of polynomials for the age covariate and whether to include it in parameters beyond μ by comparing BIC scores across various models.

Model covariates beyond age, including sex and site (considered both as a fixed effect and a random effect), are empirically selected. Each covariate is sequentially incorporated into the parameter formulas, and the resulting models are compared based on their BIC scores. The model with the lowest BIC score is chosen, determining whether the covariates are retained in the final model. The final models for spectral and connectivity features are reported in Supplementary Tables 4 and 5. See Supplementary Figs. 1, 2 and Supplementary Tables 1, 2 for an exploratory analysis of the differences in EEG feature distributions between male and female participants within each group. Additionally, statistical analysis for age and sex were applied across groups and datasets as shown in Supplementary Table 3.

Model evaluation

To evaluate the performance of our models, we examined the normalized quantile residuals. Visual inspection of the residual plots depicted in Supplementary Figs. 3 and 4 suggests that our models exhibit adequate fit and quality. Specifically, the residuals plotted against the fitted values and the index were evenly scattered around the horizontal line at 0. The kernel density estimation of the residuals displayed an approximate normal distribution, and the normal quantile-quantile (Q-Q) plots showed an approximately linear trend with an intercept of 0 and a slope of 1.

To validate the robustness of the model, we conducted a series of leave-one-study-out analyses. Specifically, we systematically excluded one dataset from the primary datasets, refitted the GAMLSS models, evaluated all model parameters, and then extracted developmental trajectories. We then compared these alternative trajectories to those derived from the 14 datasets for each feature and frequency band. Our findings showed remarkable consistency, with a very high correlation between the trajectories derived from the primary full dataset and those from the subsets (all $r > 0.88$ for spectral features, all $r > 0.90$ for FC features), even when large datasets were excluded (Supplementary Figs. 5 and 6).

Deviation and overlap maps

After parameters selection and validation, we trained GAMLSS models for each channel/connection across all frequency bands using the healthy control training group HC(train) (80% of the healthy sample). Subsequently, we projected the features data (i.e., relative power and functional connectivity values), of our clinical groups (PD, and AD) and the held-out healthy control testing group HC(test) (remaining 20% of the healthy sample), onto the corresponding models. This process enables us to generate the individual centiles and calculate the deviation scores (z-scores) using the quantile randomized residuals approach[82], for each channel/connection and each subject, resulting in an individual deviation map per subject.

An extreme deviation is defined as $|z\text{-score}| > 2$. Consequently, we derived positive and negative extreme deviation maps for z-scores >2 and < −2, respectively. We then computed the number of subjects with at least one

extreme deviation, as well as the number of extreme deviations per subject. Additionally, for each channel and location, we calculated the percentage of subjects showing extreme deviations at this specific location among those with at least one extreme deviation, which resulted in group-specific overlap maps.

We used group-based permutation tests to assess group differences in channel/connectivity-level overlap maps[16]. This involved shuffling case and control labels of individual-specific deviation maps. During each iteration, group labels were permuted, resulting in a new grouping of extreme deviation maps for each subject based on the shuffled labels. Subsequently, new overlap maps were computed for both HC(test) and clinical groups. By subtracting the surrogate HC(test) overlap map from the surrogate clinical group's overlap map, an overlap difference map for each disorder was derived. This procedure was repeated 5000 times to establish an empirical distribution of overlap difference maps under the null hypothesis of random group assignment. For each channel/connection, p values were obtained as the proportion of null values that exceeded the observed difference. Statistically significant effects were identified using two-tailed FDR correction ($p < 0.05$).

Data availability

Datasets 1, 2, 4, 11, 12, 13, and 14 are openly accessible on the OpenNeuro, OSF, and Zenodo platforms. The corresponding download links can be found in Supplementary Data 1. Access to other datasets can be made available upon request.

Code availability

Codes are available at https://github.com/MINDIG-1/NM-neurodeg. We used gamlss package in R[80] for statistical modeling, MNE-python package (https://mne.tools/stable/index.html) for EEG signal processing, and BrainNet Viewer (https://www.nitrc.org/projects/bnv/).

Received: 17 July 2024; Accepted: 8 April 2025;
Published online: 08 May 2025

References

1. Steinmetz, J. D. et al. Global, regional, and national burden of disorders affecting the nervous system, 1990–2021: a systematic analysis for the Global Burden of Disease Study 2021. *Lancet Neurol.* **23**, 344–381 (2024).
2. Vecchio, F. et al. Resting state cortical EEG rhythms in Alzheimer's disease: toward EEG markers for clinical applications: a review. In *Supplements to Clinical Neurophysiology* **62**, (ed. Clinical Neurophysiology) 223–236 (Elsevier, 2013).
3. Dennis, E. L. & Thompson, P. M. Functional brain connectivity using fMRI in aging and Alzheimer's disease. *Neuropsychol. Rev.* **24**, 49–62 (2014).
4. Li, H.-J. et al. Putting age-related task activation into large-scale brain networks: a meta-analysis of 114 fMRI studies on healthy aging. *Neurosci. Biobehav. Rev.* **57**, 156–174 (2015).
5. MacDonald, M. E. & Pike, G. B. MRI of healthy brain aging: a review. *NMR Biomed.* **34**, e4564 (2021).
6. Pini, L. et al. Brain atrophy in Alzheimer's disease and aging. *Ageing Res. Rev.* **30**, 25–48 (2016).
7. Ryman, S. G. & Poston, K. L. MRI biomarkers of motor and non-motor symptoms in Parkinson's disease. *Parkinsonism Relat. Disord.* **73**, 85–93 (2020).
8. Frisoni, G. B., Fox, N. C., Jack, C. R., Scheltens, P. & Thompson, P. M. The clinical use of structural MRI in Alzheimer disease. *Nat. Rev. Neurol.* **6**, 67–77 (2010).
9. Talwar, P., Kushwaha, S., Chaturvedi, M. & Mahajan, V. Systematic review of different neuroimaging correlates in mild cognitive impairment and Alzheimer's disease. *Clin. Neuroradiol.* **31**, 953–967 (2021).
10. Verdi, S., Marquand, A. F., Schott, J. M. & Cole, J. H. Beyond the average patient: how neuroimaging models can address heterogeneity in dementia. *Brain* **144**, 2946–2953 (2021).
11. Marquand, A. F., Rezek, I., Buitelaar, J. & Beckmann, C. F. Understanding heterogeneity in clinical cohorts using normative models: beyond case-control studies. *Biol. Psychiatry* **80**, 552–561 (2016).
12. Marquand, A. F. et al. Conceptualizing mental disorders as deviations from normative functioning. *Mol. Psychiatry* **24**, 1415–1424 (2019).
13. Bethlehem, Ra. I. et al. Brain charts for the human lifespan. *Nature* **604**, 525–533 (2022).
14. Rutherford, S. et al. Evidence for embracing normative modeling. *eLife* **12**, e85082 (2023).
15. Rutherford, S. et al. Charting brain growth and aging at high spatial precision. *Elife* **11**, e72904 (2022).
16. Segal, A. et al. Regional, circuit and network heterogeneity of brain abnormalities in psychiatric disorders. *Nat. Neurosci.* **26**, 1613–1629 (2023).
17. Wolfers, T. et al. Individual differences v. the average patient: mapping the heterogeneity in ADHD using normative models. *Psychol. Med.* **50**, 314–323 (2020).
18. Zabihi, M. et al. Fractionating autism based on neuroanatomical normative modeling. *Transl. Psychiatry* **10**, 384 (2020).
19. Wolfers, T. et al. Mapping the heterogeneous phenotype of schizophrenia and bipolar disorder using normative models. *JAMA Psychiatry* **75**, 1146–1155 (2018).
20. Verdi, S. et al. Revealing individual neuroanatomical heterogeneity in Alzheimer disease using neuroanatomical normative modeling. *Neurology* **100**, e2442–e2453 (2023).
21. Sun, L. et al. Human lifespan changes in the brain's functional connectome. *Nat. Neurosci.*, 1-11. Preprint at https://doi.org/10.1101/2023.09.12.557193 (2025).
22. Huo, Y. et al. Delineating the heterogeneity of Alzheimer's disease and mild cognitive impairment using normative models of the dynamic brain functional networks. *Biol. Psychiatry* S0006322324013659 https://doi.org/10.1016/j.biopsych.2024.05.025 (2024).
23. Lefebvre, A. et al. Alpha waves as a neuromarker of autism spectrum disorder: the challenge of reproducibility and heterogeneity. *Front. Neurosci.* **12**, 662 (2018).
24. Ebadi, A. et al. Beyond homogeneity: charting the landscape of heterogeneity in psychiatric electroencephalography. Preprint at https://doi.org/10.1101/2024.03.04.583393 (2024).
25. Chiarion, G., Sparacino, L., Antonacci, Y., Faes, L. & Mesin, L. Connectivity analysis in EEG data: a tutorial review of the state of the art and emerging trends. *Bioengineering* **10**, 372 (2023).
26. Zhang, H. et al. The applied principles of EEG analysis methods in neuroscience and clinical neurology. *Mil. Med. Res.* **10**, 67 (2023).
27. Benwell, C. S. Y. et al. EEG spectral power abnormalities and their relationship with cognitive dysfunction in patients with Alzheimer's disease and type 2 diabetes. *Neurobiol. Aging* **85**, 83–95 (2020).
28. Harada, C. N., Natelson Love, M. C. & Triebel, K. L. Normal cognitive aging. *Clin. Geriatr. Med.* **29**, 737–752 (2013).
29. Javaid, H., Kumarnsit, E. & Chatpun, S. Age-related alterations in EEG network connectivity in healthy aging. *Brain Sci.* **12**, 218 (2022).
30. Meghdadi, A. H. et al. Resting state EEG biomarkers of cognitive decline associated with Alzheimer's disease and mild cognitive impairment. *PLoS ONE* **16**, e0244180 (2021).
31. Hedden, T. & Gabrieli, J. D. E. Insights into the ageing mind: a view from cognitive neuroscience. *Nat. Rev. Neurosci.* **5**, 87–96 (2004).
32. Oschwald, J. et al. Brain structure and cognitive ability in healthy aging: a review on longitudinal correlated change. *Rev. Neurosci.* **31**, 1–57 (2019).
33. Salthouse, T. A. Selective review of cognitive aging. *J. Int. Neuropsychol. Soc.* **16**, 754–760 (2010).
34. Al-Qazzaz, N. K. et al. Role of EEG as biomarker in the early detection and classification of dementia. *ScientificWorldJournal* **2014**, 906038 (2014).

35. Chaturvedi, M. et al. Quantitative EEG (QEEG) measures differentiate Parkinsonas disease (PD) patients from healthy controls (HC). *Front. aging neurosci.* **9**, 3 (2017).
36. Lejko, N., Larabi, D. I., Herrmann, C. S., Aleman, A. & Ćurčić-Blake, B. Power and functional connectivity of alpha oscillations in mild cognitive impairment: a systematic review and meta-analysis. *Alzheimers Dement.* **16**, e040792 (2020).
37. Shirahige, L. et al. Quantitative electroencephalography characteristics for Parkinson's disease: a systematic review. *J. Parkinsons Dis.* **10**, 455–470 (2020).
38. McMackin, R., Bede, P., Pender, N., Hardiman, O. & Nasseroleslami, B. Neurophysiological markers of network dysfunction in neurodegenerative diseases. *Neuroimage Clin.* **22**, 101706 (2019).
39. Briels, C. T. et al. Reproducibility of EEG functional connectivity in Alzheimer's disease. *Alzheimers Res. Ther.* **12**, 68 (2020).
40. Pfurtscheller, G. Central beta rhythm during sensorimotor activities in man. *Electroencephalogr. Clin. Neurophysiol.* **51**, 253–264 (1981).
41. Burciu, R. G. & Vaillancourt, D. E. Imaging of motor cortex physiology in Parkinson's disease. *Mov. Disord.* **33**, 1688–1699 (2018).
42. Squire, L. R., Stark, C. E. L. & Clark, R. E. The medial temporal lobe. *Annu. Rev. Neurosci.* **27**, 279–306 (2004).
43. Engel, A. K. & Fries, P. Beta-band oscillations-signalling the status quo? *Curr. Opin. Neurobiol.* **20**, 156–165 (2010).
44. Filippi, M. et al. The human functional connectome in neurodegenerative diseases: relationship to pathology and clinical progression. *Expert Rev. Neurother.* **23**, 59–73 (2023).
45. Chen, P. et al. Robustly uncovering the heterogeneity of neurodegenerative disease by using data-driven subtyping in neuroimaging: a review. *Brain Res.* **1823**, 1–13 (2024).
46. Duara, R. & Barker, W. Heterogeneity in Alzheimer's disease diagnosis and progression rates: implications for therapeutic trials. *Neurotherapeutics* **19**, 8–25 (2022).
47. Robinson, J. L. et al. Pathological combinations in neurodegenerative disease are heterogeneous and disease-associated. *Brain* **146**, 2557–2569 (2023).
48. Vogel, J. W. et al. Connectome-based modelling of neurodegenerative diseases: towards precision medicine and mechanistic insight. *Nat. Rev. Neurosci.* **24**, 620–639 (2023).
49. Wüllner, U. et al. The heterogeneity of Parkinson's disease. *J. Neural Transm.* **130**, 827–838 (2023).
50. Hampel, H. et al. Blood-based biomarkers for Alzheimer disease: mapping the road to the clinic. *Nat. Rev. Neurol.* **14**, 639–652 (2018).
51. Young, A. L. et al. Uncovering the heterogeneity and temporal complexity of neurodegenerative diseases with subtype and stage inference. *Nat. Commun.* **9**, 4273 (2018).
52. Armstrong, R. A., Lantos, P. L. & Cairns, N. J. Overlap between neurodegenerative disorders. *Neuropathology* **25**, 111–124 (2005).
53. Jongsiriyanyong, S. & Limpawattana, P. Mild cognitive impairment in clinical practice: a review article. *Am. J. Alzheimers Dis. Other Demen.* **33**, 500–507 (2018).
54. Babiloni, C. The dark side of Alzheimer's disease: neglected physiological biomarkers of brain hyperexcitability and abnormal consciousness level. *JAD* **88**, 801–807 (2022).
55. Babiloni, C. et al. International Federation of Clinical Neurophysiology (IFCN)–EEG research workgroup: recommendations on frequency and topographic analysis of resting state EEG rhythms. Part 1: applications in clinical research studies. *Clin. Neurophysiol.* **131**, 285–307 (2020).
56. Hatlestad-Hall, C. et al. Reliable evaluation of functional connectivity and graph theory measures in source-level EEG: how many electrodes are enough. *Clin. Neurophysiol.* **150**, 1–16 (2023).
57. Allouch, S. et al. Effect of channel density, inverse solutions and connectivity measures on EEG resting-state networks reconstruction: a simulation study. *NeuroImage* **271**, 120006 (2023).
58. Bayer, J. M. et al. Site effects how-to and when: An overview of retrospective techniques to accommodate site effects in multi-site neuroimaging analyses. *Front. Neurol.* **13**, 923988 (2022).
59. Babiloni, C. et al. Measures of resting state EEG rhythms for clinical trials in Alzheimer's disease: recommendations of an expert panel. *Alzheimers Dement.* **17**, 1528–1553 (2021).
60. Babiloni, C. et al. EEG measures for clinical research in major vascular cognitive impairment: recommendations by an expert panel. *Neurobiol. Aging* **103**, 78–97 (2021).
61. Hatlestad-Hall, C. et al. Reliable evaluation of functional connectivity and graph theory measures in source-level EEG: how many electrodes are enough? *Clin. Neurophysiol.* **150**, 1–16 (2023).
62. McKhann, G. M. et al. The diagnosis of dementia due to Alzheimer's disease: recommendations from the National Institute on Aging-Alzheimer's Association workgroups on diagnostic guidelines for Alzheimer's disease. *Alzheimers Dement.* **7**, 263–269 (2011).
63. American Psychiatric Association. *Diagnostic and Statistical Manual of Mental Disorders: DSM-5*, Vol. 5 (American psychiatricassociation, 2013).
64. Daniel, S. E. & Lees, A. J. Parkinson's Disease Society Brain Bank, London: overview and research. *J. Neural Transm. Suppl.* **39**, 165–172 (1993).
65. Postuma, R. B. et al. MDS clinical diagnostic criteria for Parkinson's disease. *Mov. Disord.* **30**, 1591–1601 (2015).
66. Bigdely-Shamlo, N., Mullen, T., Kothe, C., Su, K.M. & Robbins, K.A. The PREP pipeline: standardized preprocessing for large-scale EEG analysis. *Front. neuroinformatics.* **9**, 16 (2015).
67. Pion-Tonachini, L., Kreutz-Delgado, K. & Makeig, S. ICLabel: an automated electroencephalographic independent component classifier, dataset, and website. *NeuroImage* **198**, 181–197 (2019).
68. Jas, M., Engemann, D. A., Bekhti, Y., Raimondo, F. & Gramfort, A. Autoreject: automated artifact rejection for MEG and EEG data. *NeuroImage* **159**, 417–429 (2017).
69. Yassine, S. et al. Functional brain Dysconnectivity in Parkinson's disease: a 5-year longitudinal study. *Mov. Disord.* **37**, 1444–1453 (2022).
70. Yassine, S. et al. Identification of Parkinson's disease subtypes from resting-state electroencephalography. *Mov. Disord.* **38**, 1451–1460 (2023).
71. Yassine, S. et al. Electrophysiological signatures of anxiety in Parkinson's disease. *Transl. Psychiatry* **14**, 1–11 (2024).
72. Chaturvedi, M. et al. Phase lag index and spectral power as QEEG features for identification of patients with mild cognitive impairment in Parkinson's disease. *Clin. Neurophysiol.* **130**, 1937–1944 (2019).
73. Hassan, M. & Wendling, F. Electroencephalography source connectivity: aiming for high resolution of brain networks in time and space. *IEEE Signal Process. Mag.* **35**, 81–96 (2018).
74. Pascual-Marqui, R. D. Discrete, 3D distributed, linear imaging methods of electric neuronal activity. Part 1: exact, zero error localization. *arXiv* https://doi.org/10.48550/arXiv.0710.3341 (2007).
75. Fillmore, P.T., Phillips-Meek, M.C. & Richards, J.E. Age-specific MRI brain and head templates for healthy adults from 20 through 89 years of age. *Front. aging. neurosci.* **7**, 44 (2015).
76. Desikan, R. S. et al. An automated labeling system for subdividing the human cerebral cortex on MRI scans into gyral based regions of interest. *NeuroImage* **31**, 968–980 (2006).
77. Brookes, M. J. et al. Measuring functional connectivity using MEG: methodology and comparison with fcMRI. *Neuroimage* **56**, 1082–1104 (2011).
78. Hipp, J. F., Hawellek, D. J., Corbetta, M., Siegel, M. & Engel, A. K. Large-scale cortical correlation structure of spontaneous oscillatory activity. *Nat. Neurosci.* **15**, 884–890 (2012).

79. Brookes, M. J., Woolrich, M. W. & Barnes, G. R. Measuring functional connectivity in MEG: a multivariate approach insensitive to linear source leakage. *NeuroImage* **63**, 910–920 (2012).
80. Stasinopoulos, D. M. & Rigby, R. A. Generalized additive models for location scale and shape (GAMLSS) in R. *J. Stat. Softw.* **23**, 1–46 (2008).
81. Rigby, R. A. & Stasinopoulos, D. M. Generalized additive models for location, scale and shape. *J. R. Stat. Soc. Ser. C Appl. Stat.* **54**, 507–554 (2005).
82. Dunn, P. K. & Smyth, G. K. Randomized quantile residuals. *J. Comput. Graph. Stat.* **5**, 236–244 (1996).

Acknowledgements

This work was fully funded by MINDIG as a part of its R&D activity. We would like to thank all the researchers who shared their data in open access and all the participants who approved the use of their data in research. This work was supported by the “Region Bretagne”, Inno R&D project no. 23001155 and Rennes Metropole (AICE project).

Author contributions

J.T., S.A., A.E. and M.H. conceived the study and wrote the manuscript, with valuable revision from all authors. Results were interpreted by J.T., S.A., A.M., A.E., C.B. and M.H., with contributions from all authors. A.M., M.V., B.G., G.Y., U.G., P.F. and V.P. provided datasets. A.K. and A.E. helped in the data preprocessing and analysis part.

Competing interests

The authors declare no competing interests.

Additional information

Supplementary information The online version contains supplementary material available at https://doi.org/10.1038/s41531-025-00957-6.

Correspondence and requests for materials should be addressed to Mahmoud Hassan.

Reprints and permissions information is available at http://www.nature.com/reprints

Publisher’s note Springer Nature remains neutral with regard to jurisdictional claims in published maps and institutional affiliations.

Open Access This article is licensed under a Creative Commons Attribution 4.0 International License, which permits use, sharing, adaptation, distribution and reproduction in any medium or format, as long as you give appropriate credit to the original author(s) and the source, provide a link to the Creative Commons licence, and indicate if changes were made. The images or other third party material in this article are included in the article’s Creative Commons licence, unless indicated otherwise in a credit line to the material. If material is not included in the article’s Creative Commons licence and your intended use is not permitted by statutory regulation or exceeds the permitted use, you will need to obtain permission directly from the copyright holder. To view a copy of this licence, visit http://creativecommons.org/licenses/by/4.0/.

© The Author(s) 2025